

# Hyperexcitable pyramidal neurons embedded in an inhibition-dominated network in the superficial retrosplenial cortex

Ellen Brennan<sup>1</sup>, Shyam Kumar Sudhakar<sup>1</sup>, Izabela Jedrasiak-Cape<sup>1</sup>, and Omar Ahmed<sup>1</sup>

<sup>1</sup>University of Michigan

May 2, 2019

**AUTHORS:**

Ellen K.W. Brennan<sup>1,2\*</sup>, Shyam Kumar Sudhakar<sup>1\*</sup>, Izabela Jedrasiak-Cape<sup>1</sup> & Omar J. Ahmed<sup>1,2,3,4,5</sup>

**AFFILIATIONS:**

<sup>1</sup>Dept. of Psychology,

<sup>2</sup>Neuroscience Graduate Program,

<sup>3</sup>Michigan Center for Integrative Research in Critical Care,

<sup>4</sup>Kresge Hearing Research Institute,

<sup>5</sup>Dept. of Biomedical Engineering,

University of Michigan, Ann Arbor, MI 48109.

\*Co-first authors

**CORRESPONDENCE TO:**

Omar J. Ahmed

*Mail:* Department of Psychology, 530 Church St. University of Michigan, Ann Arbor, MI 48109

*Email:* ojahmed@umich.edu

**KEYWORDS:**

neural code, memory, RSG, low rheobase, fast-spiking inhibitory, feedforward inhibition, computational model

## ABSTRACT

The retrosplenial cortex (RSC) is essential for successful memory formation and spatial navigation. However, the rate and temporal coding schemes employed by the RSC to achieve these functions remain a mystery, and no biophysically realistic computational models of RSC cells yet exist. To understand the computational principles underlying RSC function, here we systematically characterize the intrinsic physiology and local connectivity of neurons in the superficial layers of the retrosplenial granular cortex (RSG). We show that the most prominent cell type in layers 2/3 of the RSG is a hyperexcitable, small pyramidal cell. These cells have a low rheobase (LR), high input resistance, lack of spike-frequency adaptation, and spike widths that are intermediate to those of neighboring fast-spiking (FS) inhibitory neurons and regular-spiking (RS) excitatory neurons. Using paired whole-cell recordings, we show, for the first time, that these LR cells are excitatory. However, they rarely synapse onto neighboring L2/3 neurons, exciting only 17% of FS cells and 0% of other L2/3 LR or RS cells. Instead, their axons head to deeper layers and towards the corpus callosum, likely targeting contralateral RSC. LR cells receive dominant inhibition from neighboring FS cells, with FS cells inhibiting over 52% of LR cells. Given the sparsity of reciprocal LR to FS connections, this inhibition is more likely to serve a feedforward, rather than feedback, role. In terms of rhythmic computations, this also means that the superficial RSG circuit may not employ the standard rules of pyramidal-interneuron gamma (PING) generation. Our results suggest that the retrosplenial cortex uses unique coding schemes that balance hyperexcitable excitatory neurons capable of sustained long-duration firing with dominant feedforward inhibitory control.

## INTRODUCTION

The retrosplenial cortex (RSC) plays a critical role in learning, memory, and spatial navigation. In humans, damage to the RSC via hemorrhage or tumor resulted in both anterograde and retrograde amnesia spanning up to multiple years (Chrastil, 2018; Heilman and Sypert, 1977; Ironside and Guttmacher, 1929; Todd and Bucci, 2015; Valenstein et al., 1987). Similar impacts on memory are also seen in animal studies in which the RSC is lesioned or silenced. In macaque monkeys, recall of learned images as well as the ability to learn new images was impaired when the RSC was lesioned, suggesting both retrograde and anterograde amnesic effects (Buckley and Mitchell, 2016). In rodents, lesioning the RSC worsens performance on spatial learning tasks such as the Morris Water Maze and radial arm maze, and impairs conditional learning such as tone discrimination of fear conditioned responses, suggesting the RSC is necessary for normal learning (Keene and Bucci, 2008; Sigwald et al., 2016; Todd et al., 2017, 2015; van Groen et al., 2004; Vann et al., 2003; Yamawaki et al., 2019).

Apart from its well-established contributions to memory functions, the RSC is also critical for spatial navigation (Epstein, 2008; Maguire, 2001). Human case studies show that damage to the RSC leads to disorientation in space in addition to memory impairments (Bottini et al., 1990; Ino et al., 2007; Osawa et al., 2007; Takahashi et al., 1997). Such patients can identify known scenes or locations but are unable to extract any orientation or location information from them and thus experience difficulties navigating even familiar environments (Bottini et al., 1990; Ino et al., 2007; Takahashi et al., 1997). A neuroimaging study identified the coding of head direction information in the RSC while participants navigated a novel virtual environment, suggesting that the visual cues of orientation are processed in part by the RSC during navigation (Shine et al., 2016). Many animal studies also report encoding of spatial information within the RSC, including that of head direction, position, and turning behavior (Alexander & Nitz, 2015; Cho & Sharp, 2001; Vedder et al., 2016).

The RSC's role in memory and spatial navigation processes is accentuated in part by its extensive connections with other brain regions critical to these functions. Specifically, the granular region of the RSC (RSG) is highly interconnected with the subicular complex, CA1 of the hippocampus, the entorhinal cortex, and the anterior thalamic nuclei (van Groen and Michael Wyss, 1990; Van Groen and Wyss, 2003; Wyss and Van Groen, 1992). Regions "a" and "b" of RSG also have extensive connections with each other across the cortical layers and hemispheres. Despite the well-established dense connectivity of the RSC with other brain regions, the precise nature and properties of the neuronal subtypes involved in these connections is largely unknown (Sugar et al., 2011).

Layers 2/3 of the RSG consist of densely packed neurons (Kurotani et al., 2013; Michael et al., 1990). Here, we perform a detailed characterization of the local cell types within the superficial

layers of RSG to gain insight into the local connectivity of this region and decode its computational properties. We recorded from retrosplenial slice preparations of the mouse brain to characterize the intrinsic physiology of L2/3 neurons, their local synaptic connectivity, and the computational coding schemes they are capable of. We find that the majority of neurons within this region are a distinct subtype of small pyramidal neuron that are excitatory and highly intrinsically excitable but, surprisingly, very rarely excite their neighboring inhibitory or excitatory neurons. Instead, local inhibition from fast-spiking L2/3 neurons onto these highly excitable neurons is the dominant local connectivity. Our results highlight a unique cell type and connectivity pattern that is optimally suited to selectively respond to sustained high-activity input, and likely to support the learning and memory functions of the retrosplenial cortex.

## METHODS

### *Slice preparation*

All housing of animals and procedures were approved by the University of Michigan Institutional Animal Care and Use Committee. Multiple mouse lines were used in this study, including PV-IRES-Cre (Jackson Laboratories, 008069), CaMKII-Cre (Jackson Laboratories, 005359), Ai32 (Jackson Laboratories, 024109), Ai14 (Jackson Laboratories, 007914), PV-IRES-Cre x Ai14 (crossed in house), PV-IRES-Cre x Ai32 (crossed in house), CaMKII-Cre x Ai32 (crossed in house), and NTSR1-Cre (MMRRC, 030648-UCD). A total of 167 recordings are included in this study from the following mouse lines: PV-IRES-Cre (55), CaMKII-Cre (15), Ai32 (3), PV-IRES-Cre x Ai14 (3), PV-IRES-Cre x Ai32 (64), CaMKII-Cre x Ai32 (20), and NTSR1-Cre (7). Mice of both sexes between the ages of P21-31 and P62-63 were included in the experiments. No differences in cell type properties were observed across mouse lines, while both age and sex were explicitly analyzed in terms of their relationship to cell type properties (see results).

Mice underwent deep isoflurane anesthesia before decapitation. Brains were removed within one minute of decapitation and placed in an ice-cold high-sucrose slicing solution that had been saturated with carbogen gas for at least 30 minutes prior to use. Coronal slices (300µm) were cut using a Leica 1200 VT vibratome. Slices were allowed to rest in the slicing solution for about 2 minutes before being placed in a carbogen-saturated high-magnesium artificial CSF (ACSF) solution to incubate at body temperature (32°C) for 20 minutes. The entire bubbling bath was then removed from the heater, allowing the slices to gradually cool to room temperature. Slices rested an additional 30 minutes at room temperature before use.

Slices were submerged in a recording chamber with a constant flow of ACSF containing 126 mM NaCl, 1.25 mM NaH<sub>2</sub>PO<sub>4</sub>, 26 mM NaHCO<sub>3</sub>, 3 mM KCl, 10 mM dextrose, 1.20 mM CaCl<sub>2</sub>, and 1 mM MgSO<sub>4</sub>. Recordings were done between 29-31°C with an ACSF flow rate of 2 mL per minute. All recordings were done within 8 hours of slicing to ensure reputable health of the cells. Patch pipettes with 2-3 µm diameter and resistances of 3-6 M were filled with a potassium gluconate internal solution containing 130 mM K-gluconate, 2 mM NaCl, 4 mM KCl, 10 mM HEPES, 0.2 mM EGTA, 0.3 mM GTP-Tris, 14 mM phosphocreatine-Tris, and 4 mM ATP-Mg (pH 7.25, ~290 mOsm).

### *Whole-cell recordings*

Slices were visualized using the Olympus BX51WI microscope equipped with Olympus 5x and 60x water immersion lens and the Andor Neo sCMOS camera (Oxford Instruments, Abingdon, Oxfordshire, UK). In most cases, neurons were patched randomly within layers 2/3 of RSG with the exception of experiments in which PV neurons were targeted for patching based on their expression of either an eYFP tag (PV-IRES-Cre x Ai32 cross) or a tdTomato tag (PV-IRES-CRE

x Ai14 cross). All recordings were done under current clamp conditions using the Multiclamp 700B and Digidata 1400 (Molecular Devices). Neurons were adjusted for series resistances and held at a resting potential of -65 mV (unless otherwise stated) using a constant holding current injection. In order to characterize the different neuron types, intrinsic and firing properties of recorded neurons were calculated using the Clampfit and Matlab software packages.

The following intrinsic neuronal properties were calculated: resting membrane potential, spike threshold, spike amplitude, spike width, input resistance ( $R_{in}$ ), membrane time constant ( $\tau_m$ ), capacitance ( $C_{in}$ ), afterhyperpolarization (AHP) amplitude, AHP latency, spike frequency adaptation ratio, and rheobase. Resting membrane potential was recorded within 2 minutes of break-in. Cells with depolarized break-in potentials ( $> -55$  mV) were not included in this study. Spike threshold, amplitude, width, AHP amplitude, and AHP latency were calculated by average all spikes in the first sweep of a 600 ms current step protocol that elicited a firing rate of at least 5 Hz. Spike threshold is calculated from the peak of the third derivative of membrane potential (Cruikshank et al., 2012). Spike amplitude was measured as the voltage change from the spike threshold to the peak of the action potential. Spike width was calculated as the full-width at half-max of the spike amplitude. AHP amplitude was calculated as the voltage change from spike threshold to the peak negativity of the AHP, and AHP latency as the time from peak of the spike to peak negativity of the AHP. Input resistance ( $R_{in}$ ), membrane time constant ( $\tau_m$ ), and input capacitance ( $C_{in}$ ) were calculated from a series of small negative current steps ranging from -5 pA to -30 pA, creating a deflection in membrane potential of -2 to -4 mV.  $R_{in}$  was calculated using Ohm's law, as the mean voltage change divided by mean current amplitude.  $\tau_m$  was calculated by fitting a single exponential to the average of the initial 60 ms voltage response, ignoring the first 20 ms.  $C_{in}$  was then calculated from those two parameters using the formula  $\tau_m = R_{in} \times C_{in}$ . Spike frequency adaptation ratio was calculated from the first sweep of the 600ms current step protocol that elicited a firing rate of at least 10Hz (6 spikes per 600ms) using the equation  $ISI_{last} / ISI_{first}$ . Rheobase was calculated from 1 sec current pulses increasing in steps of 1-5 pA as the minimum current required to elicit at least one action potential.

A two-tailed Wilcoxon rank sum was used to compute the statistical significance between the intrinsic properties of various neuronal subtypes. To establish the statistical significance between the probability of EI and IE connections, a bootstrap resampling (1000 bootstrap samples) method was used to generate a distribution of connectivity probabilities (Sudhakar et al., 2017). Statistical significance was then computed using two-tailed t-test with a confidence interval of 95%.

#### *Optogenetic testing of CaMKII expression*

Optogenetic verification of CaMKII expression was conducted using CaMKII-Cre x Ai32 mice (Jackson Laboratories 005359 and 024109 respectively, crossed in house) in which channelrhodopsin is expressed in CaMKII-Cre-expressing neurons. Slices were visualized with the Olympus BX51WI equipped with Olympus 5x and 60x water immersion lens. Expression of channel-

rhodopsin was marked by fluorescence of the eYFP tag. Neurons were recorded in the same manner as described above with at least one additional protocol to verify functional expression of the channelrhodopsin. One millisecond optogenetic light pulses with a 5,500K white LED ((Mightex; 14.47 mW)) were delivered at 10 Hz while the neuronal responses were recorded. Direct expression was verified by responses to the light pulses under 0.5 ms.

#### *Morphological investigations with biocytin*

To determine patched cells' morphology, 5mg/ml of biocytin was added to the internal solution of recording electrodes. Cells were filled with biocytin (Sigma, cat. no. B4261) throughout the recording session, and the pipette was left attached to the cell for at least 20min. At the end of the recording, cells were "zapped" with fifteen 1 Hz pulses of 3-4 nA current to improve the diffusion of biocytin into the axon (Jiang et al., 2015). Slices were left to recover in the recording chamber for 30 min before further processing. A detailed description of the biocytin labelling and processing is available elsewhere (Marx et al., 2012). Briefly, slices were filled with biocytin as described above, placed in 4% paraformaldehyde for 12-15 hours, and then transferred to phosphate buffer solution (PBS). After 24-48 hours in the PBS, slices were incubated in avidin-biocytin (ABC Elite kit, VectaShield) for 12 hours and then treated with peroxidase to reveal cell morphology. Finally, slices were mounted on microscope slides with Mowiol-based embedding medium and allowed to dry for at least 12 hours. Cells were visualized using a Leica DM4000B light microscope equipped with a Leica DMC 6200 CMOS camera.

## RESULTS

### Low Rheobase cells are highly excitable neurons in the superficial retrosplenial granular cortex

We recorded from 167 cells in the superficial layers (L2/3) of the mouse retrosplenial granular cortex (RSG). Consistent with other cortical regions, fast-spiking (FS) interneurons were present in these RSG layers (Figure 1A). FS cells were identified by their unique spiking properties (Sempere-Ferrandez et al., 2018), including their narrow spike width and rapid, sharp AHPs. Regular-spiking (RS) pyramidal neurons were occasionally found, but far less often than in typical neocortex (Figure 1B). A third population of cells was identified with distinct and unique physiological and intrinsic properties. The action potentials of these neurons were narrower than typical RS cells and often displayed prominent afterdepolarizations (Figure 1C). Detailed analyses of physiological and intrinsic parameters revealed several distinct and unique properties of these neurons. Spike widths were between those of FS and RS cells (FS =  $0.22 \pm 0.05$  ms, RS =  $0.86 \pm 0.05$  ms, LR =  $0.55 \pm 0.02$ ms;  $p < 0.01$  for each comparison; Figure 1D; Table 1). Additionally, these cells had uniquely high input resistance ( $402.69 \pm 16.75$  M;  $p < 0.01$ ), low input capacitance ( $38.42 \pm 1.32$  pF;  $p < 0.01$ ), and low rheobase ( $91.79 \pm 12.89$  pA;  $p < 0.01$ ), suggesting they are a class of highly excitable neurons compared to both FS and RS neurons (Figure 1E,F,G; Table 1). They also exhibited minimal spike frequency adaptation (ratio of  $1.26 \pm 0.06$ ), far lower than the substantial spike frequency adaptation shown by RS cells (ratio of  $3.42 \pm 0.58$ ;  $p < 0.01$ ), highlighting their potential ability to fire trains of action potentials at high frequencies with minimal adaptation (Figure 1J; Table 1). For reasons investigated and explained in detail below, we refer to these unique neurons as Low Rheobase (LR) cells in the rest of this manuscript.

**Table 1. Intrinsic cell properties**

	FS	(n)	RS	(n)	LR	(n)
Postnatal age at time of recording (days)	$25.93 \pm 0.43$	(42)	$26.50 \pm 0.63$	(17)	$27.39 \pm 0.64$	(108)
Resting potential (mV)	$-61.17 \pm 0.88$	(42)	$-63.80 \pm 0.99$	(17)	$-66.41 \pm 0.67$	(108)
Input resistance (M $\Omega$ )	$64.68 \pm 5.04$	(28)	$131.27 \pm 13.01$	(15)	$402.69 \pm 16.75$	(77)
Input capacitance (pF)	$118.83 \pm 7.19$	(28)	$133.92 \pm 12.85$	(15)	$38.42 \pm 1.32$	(77)
Membrane time constant (ms)	$7.16 \pm 0.58$	(28)	$15.72 \pm 0.92$	(15)	$14.29 \pm 0.38$	(77)
Action potential threshold (mV)	$-40.73 \pm 0.85$	(35)	$-40.47 \pm 1.00$	(17)	$-40.76 \pm 0.37$	(93)
Action potential amplitude (mV)	$56.86 \pm 1.59$	(35)	$72.77 \pm 2.88$	(17)	$64.04 \pm 1.06$	(93)
Action potential width (ms)	$0.22 \pm 0.05$	(35)	$0.86 \pm 0.05$	(17)	$0.55 \pm 0.02$	(93)
Afterhyperpolarization amplitude (mV)	$17.00 \pm 0.54$	(35)	$9.52 \pm 0.44$	(17)	$11.02 \pm 0.31$	(93)
Afterhyperpolarization latency (ms)	$0.60 \pm 0.02$	(35)	$30.05 \pm 2.79$	(17)	$1.42 \pm 0.09$ (ADP)	(61)
					$9.17 \pm 0.50$ (no ADP)	(32)
Spike frequency adaptation ratio	$0.92 \pm 0.14$	(35)	$3.42 \pm 0.58$	(17)	$1.26 \pm 0.06$	(93)
Latency to first spike (ms)	$626.19 \pm 53.63$	(35)	$389.50 \pm 59.65$	(17)	$501.79 \pm 17.86$	(93)
Rheobase (pA)	$359.87 \pm 26.70$	(42)	$126.27 \pm 13.66$	(17)	$91.79 \pm 12.89$	(108)

**Table 1. Intrinsic cell properties reveal that LR cells have a uniquely low rheobase, high input resistance, low input capacitance, and low spike frequency adaptation, as well as a spike width between that of FS and RS cells. Values are means  $\pm$  SEM for each of the calculated intrinsic cell properties separated by cell group. Ns are reported individually for each property for each cell type. Details of the measurements are described in Materials and**

*Methods. LR cells significantly differed from RS cells on the following measures: input resistance, input capacitance, spike width, spike frequency adaptation ratio, and rheobase ( $p < 0.01$ ) as well as latency to first spike ( $p < 0.05$ ). LR cells significantly differed from FS cells on the following measures: input resistance, input capacitance, membrane time constant, spike width, first spike latency, AHP amplitude, and rheobase ( $p < 0.01$ ), as well as spike frequency adaptation ratio ( $p < 0.05$ ). FS: Fast-spiking; RS: Regular-Spiking; LR: Low Rheobase.*

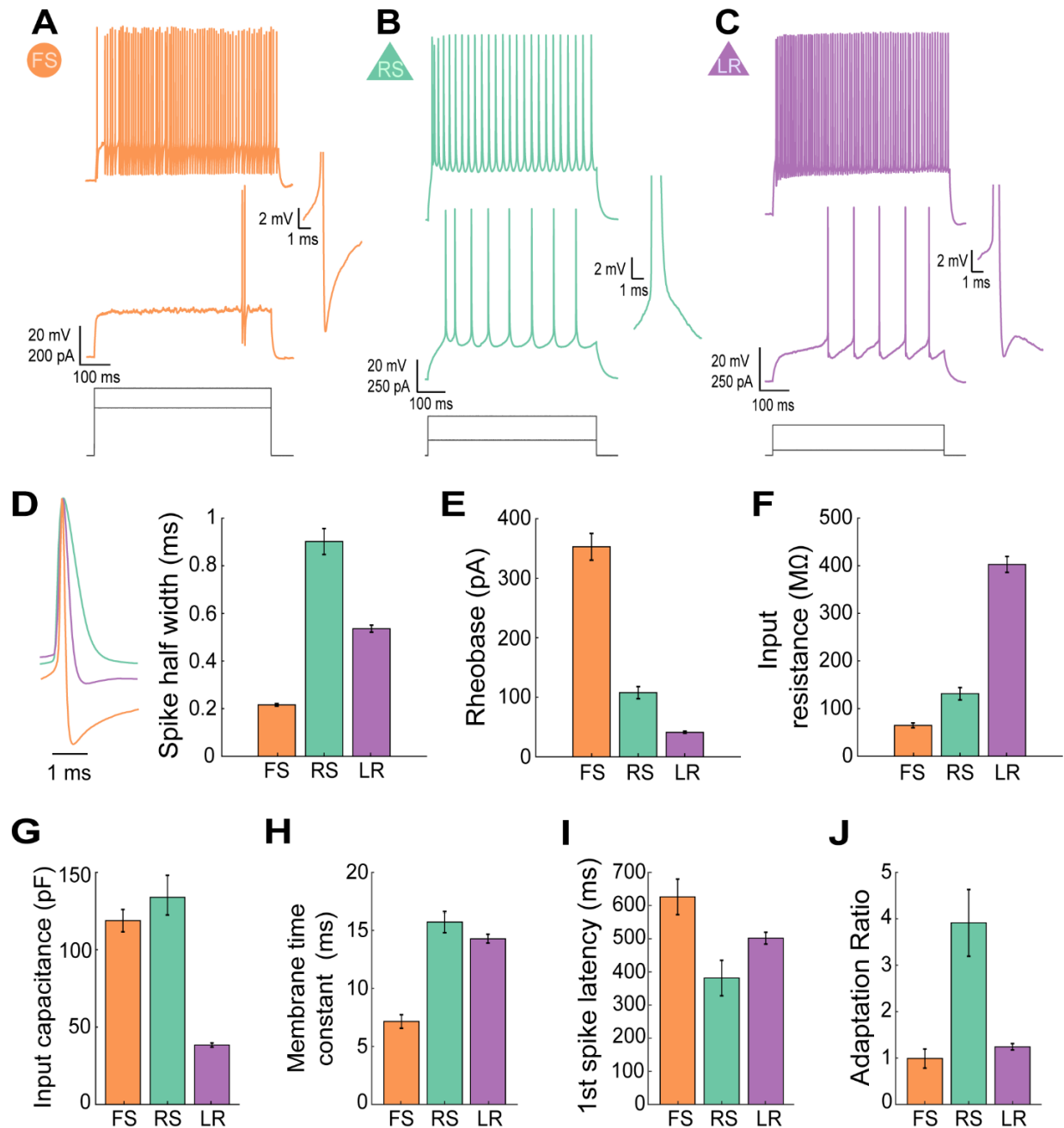


**Figure 1. Low rheobase cells represent a highly excitable cell type in the superficial retrosplenial cortex.** **A.** *Intrinsic physiological properties of an FS neuron in the superficial layers of the granular retrosplenial cortex. Top trace, Ability to fire sustained high frequency trains of action potentials with little or no spike frequency adaptation. Middle trace, A substantial delay to first spike after current onset during a near-threshold current step. This late-spiking feature was consistent across all 42 recordings of FS cells in these layers. Right inset is a zoomed-in view of the first spike in the middle trace. It shows a narrow spike width followed by a large afterhyperpolarization. These features are distinctive of FS cells and were also consistent across*

all 42 recordings of FS cells in these layers. Bottom, injected current amplitudes for the voltage responses shown above. B. Intrinsic physiological properties of an RS neuron in the superficial layers of the granular retrosplenial cortex. Top trace, Presence of spike frequency adaptation when firing at higher frequencies in response to large suprathreshold current steps. This feature was consistent across all 17 recordings of RS cells in these layers. Middle trace, Minor delay to first spike after current onset during an at-threshold current step. Right inset is a zoomed-in view of the first spike in the middle trace. It shows a relatively wide spike width followed by a gradual return to baseline membrane potential. Bottom, injected current amplitudes for the voltage responses shown above. C. Intrinsic physiological properties of an LR neuron in the superficial layers of the granular retrosplenial cortex. Top trace, Ability to fire sustained high frequency trains of action potentials with little spike frequency adaptation. Middle trace, Moderate delay to first spike after current onset during an at-threshold current step. These features were consistent across the 108 recordings of LR cells in these layers. Right inset is a zoomed-in view of the first spike in the middle trace. It shows a moderate spike width followed by a clear afterdepolarization before returning to baseline membrane potential. This afterdepolarization was present in 66% of LRs recorded in these layers ( $n=61/93$ ). Bottom, injected current amplitudes for the voltage responses shown above. D. Representative traces from FS, RS, and LR cell action potentials overlaid to show differences in spike width. Bar graph of the average spike widths for FS, RS, and LR cells showing a clear distinction between the three (error bars are standard error). E. Bar graph of the average rheobase for FS, RS, and LR cells showing a markedly low rheobase for LR cells compared to that of FS and RS (error bars are standard error). F. Bar graph of the average IR for FS, RS, and LR cells showing a uniquely high IR for LR cells (error bars are standard error). G. Bar graph of the average IC for FS, RS, and LR cells showing a markedly low IC for LR cells compared to FS and RS (error bars are standard error). H. Bar graph of the average membrane time constant ( $\tau$ ) for FS, RS, and LR cells (error bars are standard error). I. Bar graph of the average latency to first spike after onset of an at-threshold current injection for FS, RS, and LR cells showing a substantial latency to first spike for both FS and LR cells in these layers (error bars are standard error). J. Bar graph showing the average spike frequency adaptation ratio for FS, RS, and LR cells showing lack of adaptation in FS and LR cells (error bars are standard error).

In order to determine whether the LR neurons are a truly distinct cell type, we sought to identify the physiological properties that can clearly distinguish them from other neurons in the superficial RSG. Specifically, using features such as rheobase, input capacitance, input resistance, and spike width, we were able to isolate the LR cells from both FS and RS cells (Figure 2). LR cells cluster clearly and separately from FS and RS cells based on these intrinsic properties, suggesting they are a unique and distinct subtype of neuron compared to the others included in this study.

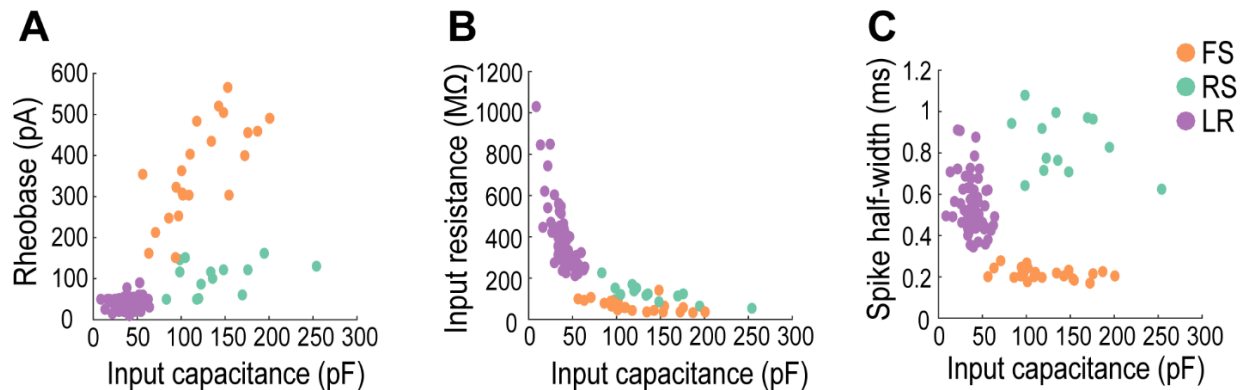


**Figure 2. Low Rheobase neurons are a distinct, unique cell type.** **A.** LR cells cluster clearly and separately from FS and RS cells when plotted against rheobase and input capacitance. **B.** LR cells cluster clearly and separately from FS and RS cells when plotted against input resistance and input capacitance. **C.** All cell groups cluster clearly and separately from each other when plotted against spike width and input capacitance.

### Low Rheobase cells are the dominant cell type in superficial retrosplenial granular cortex

LR neurons were the most commonly encountered cell type in L2/3 of RSG. To quantify the relative percentage of neurons in the superficial RSG, the recorded neurons were assigned to one of four groups based on their intrinsic physiological properties: FS, RS, LR, and unclassified. The unclassified group consisted of neurons whose intrinsic and/or firing properties did not fall under any of the three defined groups. Thus, this group includes other neuronal subtypes not investigated in this study as well as a few potential FS, RS, and LR neurons whose properties were difficult to classify. We found that LR cells are the dominant cell type in both layers 2 and 3, accounting for 51.9% of the neurons in layer 2 and 57.14% in layer 3 (Figure 3). However, 0 out of 25 recordings in layers 5 and 6 were of LR cells, suggesting that LR neurons are restricted to the superficial layers of RSG (data not shown). Surprisingly, the prevalence of RS cells in L2/3 of RSG was strikingly low, representing only 18.5% of all layer 2 neurons and 8.9% of layer 3 neurons. The FS probabilities are slightly skewed, as experiments detailed later in this manuscript specifically targeted FS interneurons. Thus, their probability reported here is likely slightly larger than their true representation in the cortex. Nonetheless, it is clear that LR cells are the most

prevalent cell type within the superficial layers of the granular retrosplenial cortex.

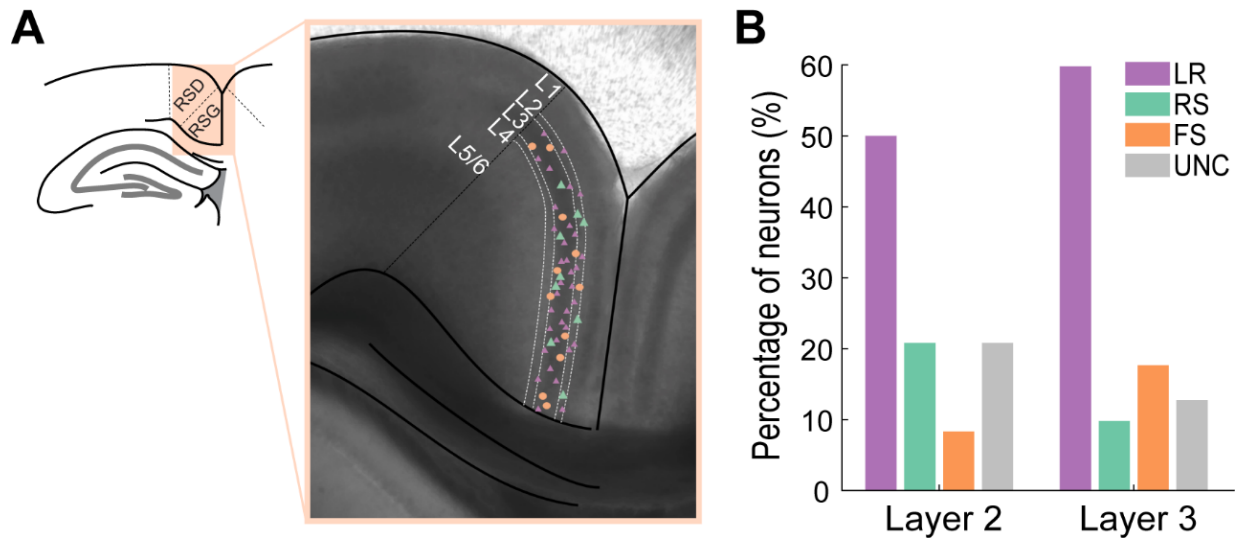


**Figure 3. LR cells are the dominant cell type in layers 2/3 of the granular retrosplenial cortex.** **A.** Representative anatomy of the RSG and locations of a subset of patched neurons. The left panel shows the location of the retrosplenial cortex superior to the corpus callosum. RSD and RSG are distinct regions within the retrosplenial cortex with RSD being more superior and lateral and RSG inferior and medial. Right panel shows a DIC image of a retrosplenial mouse brain slice with RSD and RSG separated by a black dotted line. The layers are demarcated by white dotted lines. Small purple triangles, large green triangles, and orange circles denote representative patch locations of roughly one-half of LR, RS, and FS cells patched in this study, respectively. **B.** Bar graph of the percentage of each neuron type patched in each layer of RSG. LR cells are the most prevalent cell type in each layer. UNC stands for unclassified – this group consists of other cell types within this region and neurons that were unable to be classified into one of the other three groups based on their physiological and intrinsic properties.

### Low Rheobase cells are found across the long-axis of the retrosplenial cortex

The retrosplenial cortex is a large structure, spanning 4.38 mm rostracaudally in mice. In addition to LR cells being the most prevalent cell type, we also found that their expression is consistent across this entire long axis of the retrosplenial cortex (Figure 4B). This suggests that the computational function of LR cells is likely to be similar across the long axis of the RSG.

### Low Rheobase cells are found in both males and females at all ages examined

LR cells are present in both adolescent and adult mice, suggesting this highly intrinsically excitable cell is not a transient developmental phenotype (Figure 4A). LR cells are found in both male and

female mice (Figure 4C). Thus, these neurons are the dominant cell type in the superficial granular retrosplenial cortex, consistent across age, sex, and long-axis of the RSG.

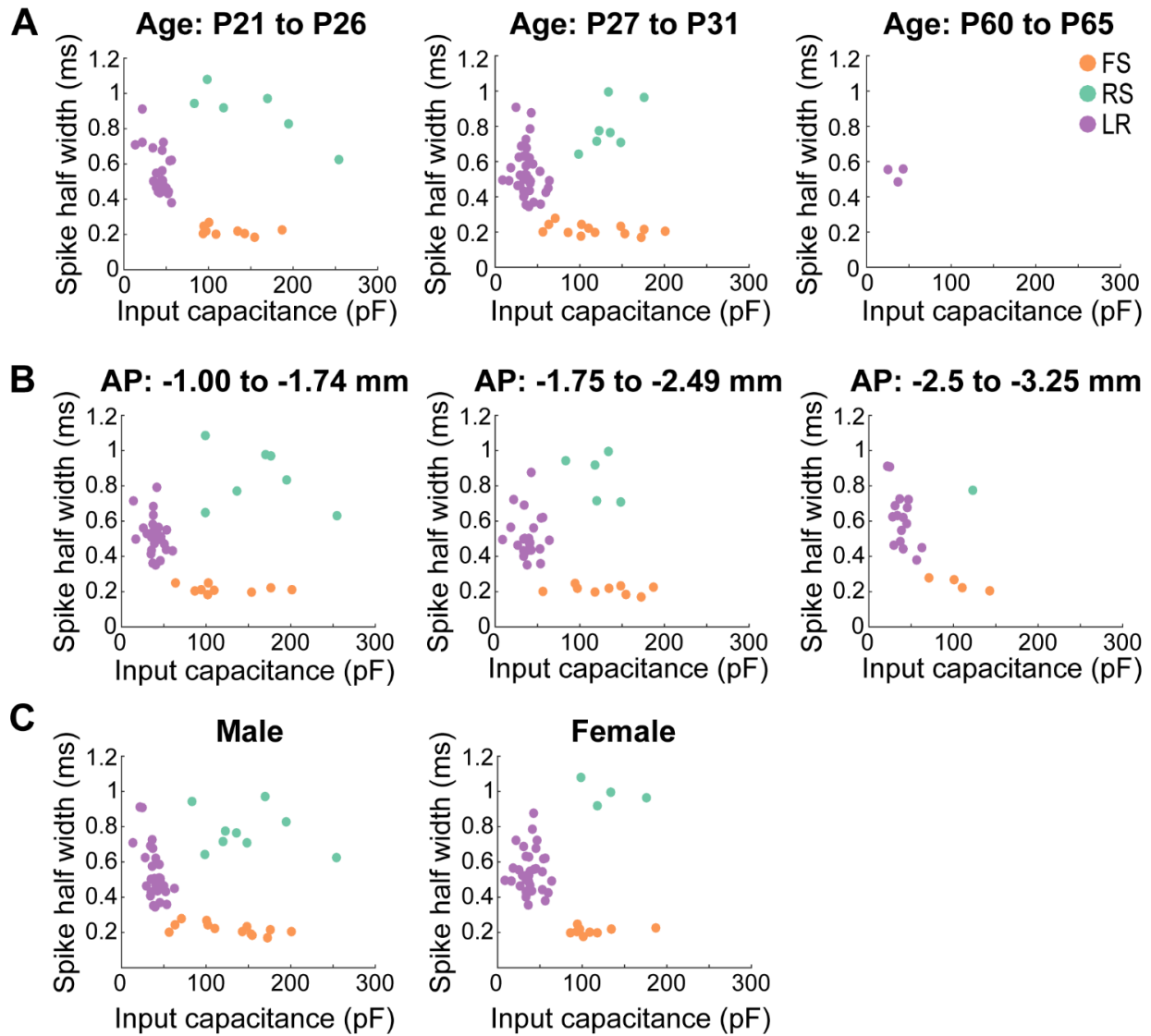


**Figure 4. LR cells are consistent across age, sex, and long-axis of the RSG. A.** Scatterplots of the three cell types plotted against spike width and input capacitance across different age groups. Left panel, Postnatal days 21-26 show consistent clustering between the three cell groups (FS:  $n = 9$ ; RS:  $n = 6$ ; LR:  $n = 22$ ). Middle panel, Postnatal days 27-31 show consistent clustering between the three cell groups (FS:  $n = 13$ ; RS:  $n = 7$ ; LR:  $n = 46$ ). Right panel, Postnatal days 60-65 show presence of LR cells in adult mice ( $n = 3$ ) clustering similarly to those recorded in adolescent mice. **B.** Scatterplots of the three cell types plotted against spike width and input capacitance across the anterior-posterior plane of the RSG. Left panel, -1 to -1.74 mm from bregma show consistent clustering between the three cell groups (FS:  $n = 9$ ; RS:  $n = 7$ ;

LR:  $n = 27$ ). Middle panel,  $-1.75$  to  $-2.49$  mm from bregma show consistent clustering between the three cell groups (FS:  $n = 9$ ; RS:  $n = 5$ ; LR:  $n = 24$ ). Right panel,  $-2.5$  to  $-3.25$  mm from bregma show consistent clustering between the three cell groups (FS:  $n = 4$ ; RS:  $n = 1$ ; LR:  $n = 17$ ). C. Scatterplots of the three cell types plotted against spike width and input capacitance across sex. Left panel, All three cell types exist and cluster consistently in male mice (FS:  $n = 13$ ; RS:  $n = 9$ ; LR:  $n = 32$ ). Right panel, All three cell types exist and cluster consistently in female mice (FS:  $n = 9$ ; RS:  $n = 4$ ; LR:  $n = 36$ ).

### Low Rheobase cells are excitatory

In order to investigate whether LR neurons were excitatory or inhibitory, we next conducted whole-cell recordings coupled with optogenetic activation of channelrhodopsin in CaMKII<sup>+</sup> cells. CaMKII-Cre x Ai32 mice (Jackson Laboratories 005359 and 024109 respectively, crossed in house) were used for these experiments. In these mice, cells containing the excitatory marker CaMKII express Cre, thus allowing for expression of a cre-dependent channelrhodopsin (ChR2) exclusively in CaMKII neurons (Figure 5A). We then used 1 ms light pulses in a 10 Hz train to test ChR2 responses in the patched neurons. Of 20 LR cells tested, 85% (17/20) directly responded to the optogenetic light pulse, indicating that they were directly expressing ChR2 and thus were CaMKII positive (Figure 5B&C). This suggested that they may be excitatory neurons.

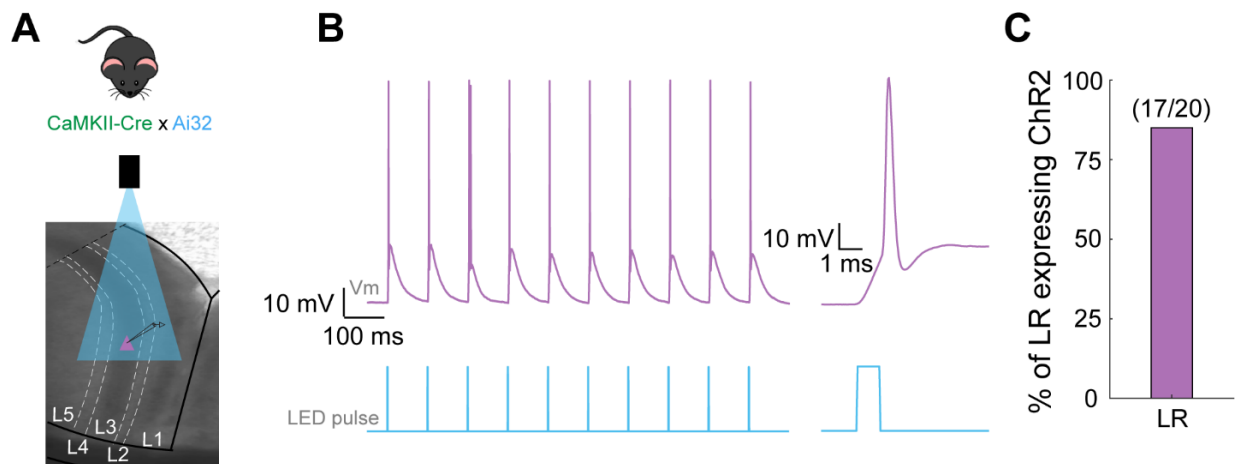


**Figure 5. LR cells directly respond to ChR2 in CaMKII-Cre x Ai32 mice, indicating expression of CaMKII in this cell type.** A. Schematic showing the experimental set-up. Top panel, Mouse indicating the genetic cross of CaMKII-Cre (Jackson Laboratories, 005359) and Ai32 (Jackson Laboratories, 024109) on a C57Bl6 background (crossed in house). Bottom panel, Schematic of the experimental set up. 10 Hz LED pulses were delivered to layers 2 and 3 of the RSG while the responses of whole-cell patched neurons were recorded. B. Representative responses of LR cell to the 10 Hz opto LED pulses. Left traces show all 10 opto LED pulses (1ms each) over the span of one second and the patched LR cell spiking one to two times in response

to each 1ms LED pulse. Right trace is a zoomed in view of the first LED pulse and respective spike from the LR cell. The neuron response to the light almost instantaneously, indicating a direct response by ChR2. C. Bar graph representing the percentage of LR cells tested that directly expressed ChR2 (85%, 17/20).

We then confirmed the excitatory nature of LR cells using paired recordings of layer 2/3 RSG neurons. Although connections were rare, when LR cells were connected to neighboring cells, they led to excitatory post-synaptic potentials (EPSPs) in their paired FS cell (Figure 6D). This is the first demonstration that LR cells in RSG are indeed excitatory neurons.

### **Dominant inhibition and rare local excitation in the superficial layers of RSG**

Using paired whole-cell recordings, we sought to quantify the connectivity between these three major cell types in the superficial layers of RSG: LR and RS (both excitatory; E) and FS (the major inhibitory neurons in these layers; I). To our surprise, LR to FS connectivity was extremely rare (17%), suggesting a lack of locally driven excitation of FS cells. On the other hand, FS cells were frequently connected to, and inhibited, neighboring LR cells (52%) (Figure 6A). When all pairs were considered, the EI connectivity was only 16%, whereas the IE connectivity reached 53% (Figure 6B). The difference in probability to observe IE connections versus EI connections was significant ( $p < 0.01$ ), suggesting the superficial layers of the RSG represents an inhibition-dominated network. Additionally, we observed no LRLR connections (0/36), nor any connectivity between LR and RS cells (0/6), indicating a complete lack of EE connectivity. II pairs were not sampled.

The amplitudes of the evoked responses from a holding potential of -55 mV were similar between inhibition and excitation (Figure 6E). However, the latency to peak was smaller in LRFS connections compared to FSLR connections. IPSPs from FS to LR cells exhibited clear short-term depression. This was seen in paired recordings (Figure 6C&H) and also when recording from LR neurons during optogenetic stimulation of FS cells (data not shown). EPSPs from LR to FS cells did not exhibit either depression or facilitation (Figure 6D&I).

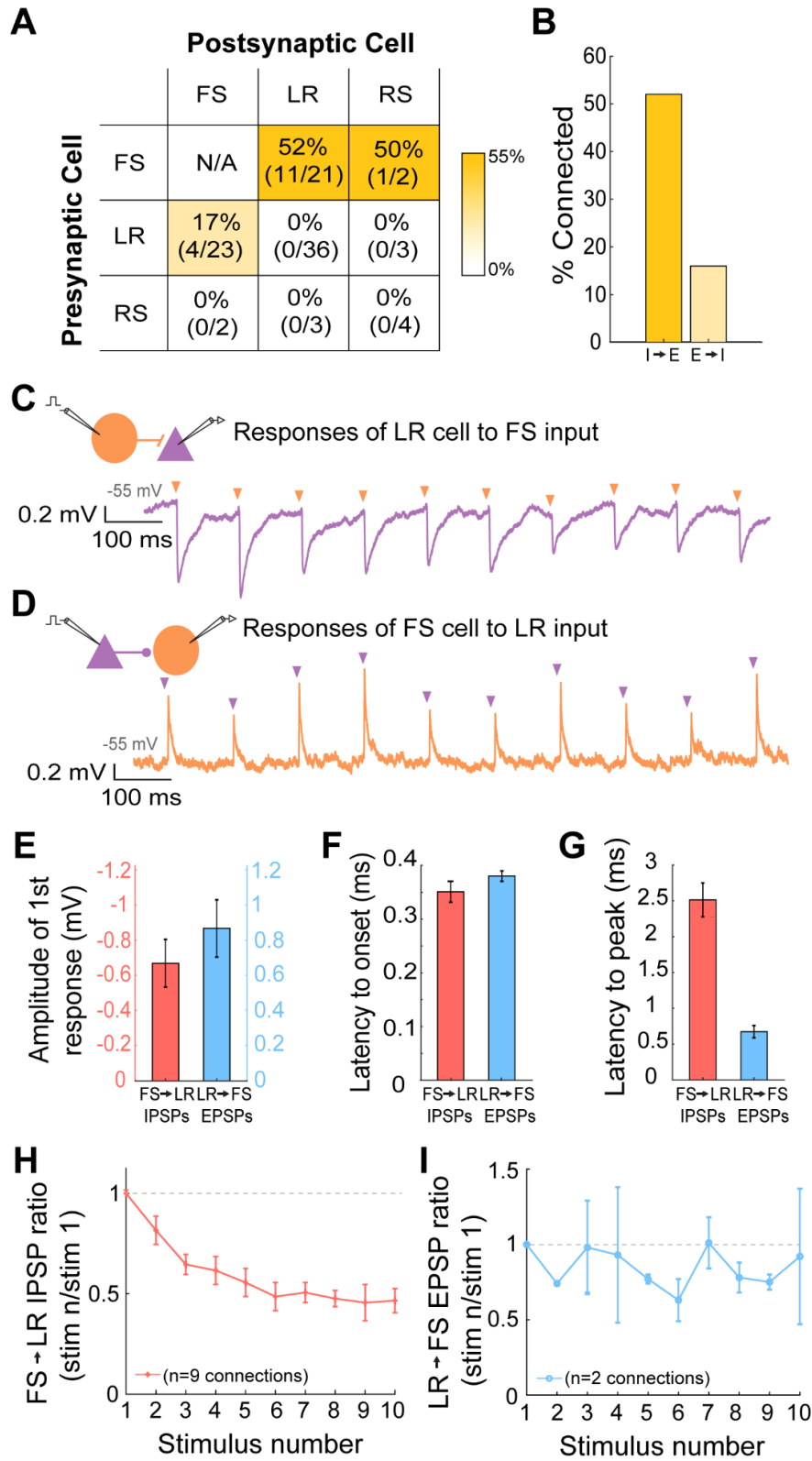


Figure 6. Dominant local inhibition in the superficial layers of the retrosplenial cortex.

**A.** Table indicating the percentage of connectivity between all types of pairs tested. No FS-FS pairs were tested in this study. FSLR connections existed in 11 of the 21 pairs recorded (52%). FSRS connections existed in 1 of the 2 pairs recorded (50%). LRFS connections existed in 4 of the 23 pairs recorded (17%). There were no RSFS connections recorded and no EE connections recorded (LRLR, LRRS, RSLR, RSRS). The heat map to the right indicates the probability of connections between the neuron types indicated in each cell of the table. Deeper gold indicates connection probabilities of near 50%, while lighter gold indicates lower probabilities and white indicates a connection probability of 0. **B.** Bar graph representing the total connectivity probability between all inhibitory to excitatory directional pairs (52%) and all inhibitory to inhibitory directional pairs (16%). Bootstrap resampling followed by a t-test revealed a significant difference in probability to observe IE connections versus EI connections. **C.** Representative trace of the connection between a layer 3 FS cell (held at -65 mV) and layer 3 LR cell (held at -55 mV). The neurons were 27  $\mu$ m apart with the LR cell located superficial to the FS cell. Schematic shows the patched pair in which the FS cell is being stimulated to spike at 10 Hz and the responses of the LR cell are being recorded. The purple trace is the responses of the LR cell to each FS cell spike (indicated by the orange arrows). **D.** Representative trace of the connection between a layer 3 LR cell (held at -65 mV) and layer 3 FS cell (held at -55 mV). The neurons were 80  $\mu$ m apart with the LR cell located superficial to the FS cell. Schematic shows the patched pair in which the LR cell is being stimulated to spike at 10 Hz and the responses of the FS cell are being recorded. The orange trace is the responses of the FS cell to each LR cell spike (indicated by the purple arrows). **E.** Bar graph showing the average amplitude of the IPSPs recorded from the FSLR pairs (red) and the EPSPs recorded from the LRFS pairs (blue). Error bars are standard error. **F.** Bar graph showing the average latency to onset of the IPSPs recorded from the FSLR pairs (red) and the EPSPs recorded from the LRFS pairs (blue). Error bars are standard error. Latency to onset was calculated as the time from the peak of the presynaptic action potential to the beginning of the postsynaptic IPSP/EPSP. **G.** Bar graph showing the average latency to peak of the IPSPs recorded from the FSLR pairs (red) and the EPSPs recorded from the LRFS pairs (blue). Error bars are standard error. Latency to peak was calculated as the time from the onset of the postsynaptic IPSP/EPSP to the peak of the postsynaptic IPSP/EPSP. **H.** Group synaptic dynamics for FSLR connections ( $n=9$ ). Inhibition onto LR cells exhibited strong short-term depression. **I.** Group synaptic dynamics for LRFS connections ( $n=2$ ). Excitation onto FS cells did not exhibit short-term depression or facilitation.

### **Axons from LR cells do not ramify locally but head to deeper layers and towards the corpus callosum**

The rarity of connections from LR neurons onto their neighboring L2/3 cells suggested that LR axons have more distant targets. In order to investigate the projections of the LR cells, we used biocytin to fill cells for morphological consideration after characterizing their physiological properties. Of the 3 LR neurons whose cell body, dendrites, and axons were sufficiently filled, all exhibited projections to the deeper layers of RSG (Figure 7A,B,D). Of the three, one axon clearly entered and traveled within the corpus callosum (Figure 7A&C). Additionally, LR neurons had

very few axonal ramifications within layers 2/3, matching their extremely low likelihood to synapse onto local neurons (Figure 7A&D). Upon further examination of our four paired recordings in which LR cells did directly excite the paired FS cell, we noticed that all of these LR cells were located more superficially than their paired FS cell. Additionally, of the four pairs in which the FS cell was located more superficial to the LR cell, none exhibited connections from the LR to the FS cell. This supports the finding that LR axons travel to deeper areas and do not ramify locally. It also suggests that FS cells in L2, even more so than L3 FS cells, are likely to be completely devoid of local excitation from LR cells.

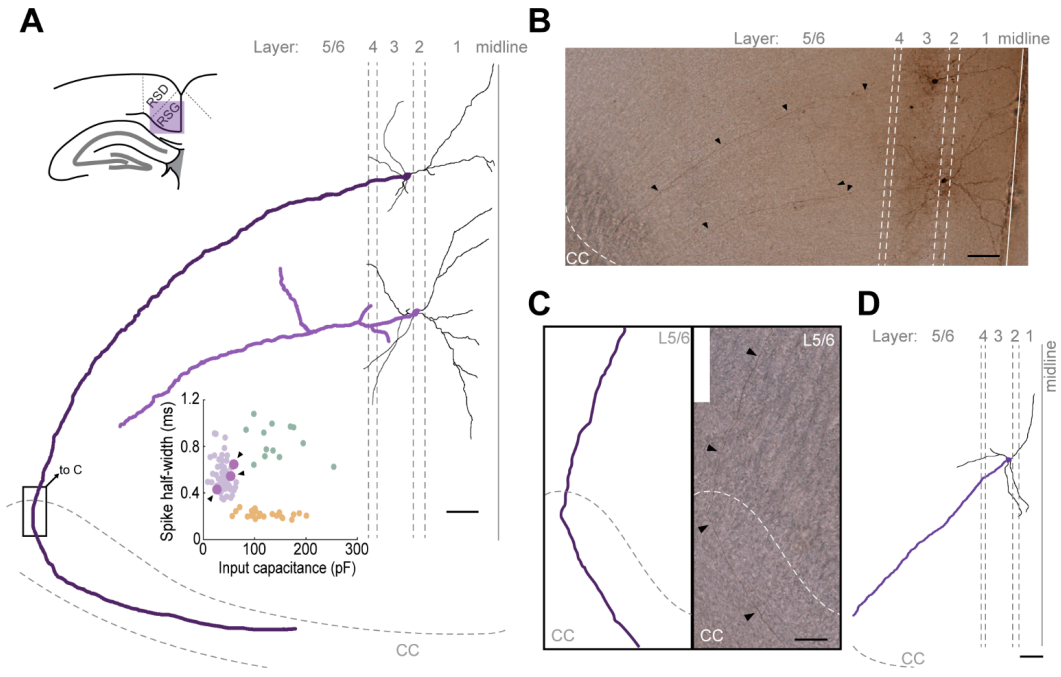


**Figure 7. LR axons do not ramify locally and instead project to deeper layers and the corpus callosum.** **A.** Schematic of the axonal ramifications of two LR neurons whose cell bodies are located within L2/3. Top left shows the location of the RSC within the slice. A slice with an anterior-posterior location of -1.82 mm was used in a P25 mouse. Layers and corpus callosum (CC) are demarcated by grey dashed lines, with the midline of the brain demarcated as a solid line. Scale bar represents 50  $\mu$ m. Dendrites are in black, and cell bodies/axons are in purple. Axons project clearly to deeper layers, with one entering the corpus callosum. Minimal axonal ramifications are observed in L2/3. Graphical insert is identical to that in Figure 2C with the three LR cells referenced here in larger purple dots, indicated by the arrows. All three LR cells cluster clearly within the LR cell group and separate from RS and FS cell groups. **B.** Biocytin fill used to create the schematic in A. Layers and the CC are demarcated by dashed lines, and the midline is a solid line. Arrows are placed periodically along the axon for visualization. Scale bar represents 50  $\mu$ m. **C.** Zoomed in view of the indicated box in A. Left shows a schematic of the axon projecting through L5/6 before entering and traveling within the CC. Right shows biocytin fill image. Arrows are placed periodically along the axon for visualization. Scale bar represents

50  $\mu\text{m}$ . D. Schematic of the third filled LR cell dendrites, cell body, and axon. A slice with an anterior-posterior location of -2.54 mm was used in a P24 mouse. Layers and corpus callosum are demarcated by grey dashed lines; a solid line indicates the midline. There are no axonal ramifications in the superficial layers, and the axon projects into deeper layers towards the corpus callosum. Scale bar represents 100  $\mu\text{m}$ .

## DISCUSSION

We have characterized the connectivity of a class of hyperexcitable excitatory pyramidal neurons existing within the superficial layers of the granular retrosplenial cortex. These neurons are excitatory (Figures 5, 6) and are the most prevalent cell type in this region (Figure 3), yet they make few local connections (Figure 6), instead sending their axons into the deeper layers and corpus callosum (Figure 7). However, they receive numerous inhibitory inputs from the neighboring FS cells (Figure 6) and thus are embedded within an inhibition-dominated network.

### **Unique intrinsic properties of Low Rheobase (LR) cells**

LR cells in the RSG have intrinsic properties that differ substantially from those of neighboring RS cells. Most importantly, and the reason we have suggested their name, is that they fire in response to very little current input, i.e. they have a low rheobase. This is dependent on their large input resistance, which in turn is most likely related to their small soma size and relatively sparse dendritic tree. LR cells also demonstrate a late-spiking phenotype in response to near-threshold current injections (Kurotani et al, 2013). Based on our findings, we argue that the late-spiking behavior of these neurons is not their most unique or defining feature. FS cells and many RS cells in the RSG also show late-spiking behavior in response to near-threshold stimuli (Figure 1). Additionally, the name “late-spiking (LS) neuron” is already most often attributed to neurogliaform cells, inhibitory interneurons found in the superficial layers of the neocortex, including layer 1 (Cruikshank et al., 2012). Instead, the intrinsic excitability of LR neurons, facilitated mostly by their high input resistance and low rheobase, is their most distinct feature and is critical to their potential computational functions. In addition, their lack of spike frequency adaptation suggests an ability to respond to high frequency inputs far more reliably than RS cells can. This, coupled with their low rheobase, makes them a rare and unique class of neurons that can respond to both weak inputs as well as sustained or high frequency inputs, thereby possessing the ability to transfer the incoming synaptic inputs to their post-synaptic targets with a high degree of precision. Thus, the name Low-Rheobase (LR) is indicative of both their unique properties compared to other cell types in this region as well as the computational functions that they are likely to perform in this circuit.

### **Sparse local excitation from LR cells**

Our study shows that while these LR cells are the most prevalent cell type in the superficial layers of the RSG, they rarely synapse onto their neighboring FS, RS and LR neurons. We have confirmed that the most likely reason for this sparse connectivity is because the axons of LR cells rarely ramify within L2/3, but instead travel into deeper layers and the corpus callosum.

Similar axonal trajectories for RSG neurons are likely to exist in both mice and rats (Kurotani et al., 2013). In additional related work, when pyramidal neurons in the superficial layers of one RSC hemisphere were labeled, their axons very often terminated in the contralateral RSC (Gejjo-barrientos et al., 2019; Sempere-Ferràndez et al., 2018). These studies did not identify whether LR or RS neurons were the more likely source of these projections, but combined with our results, suggest a circuit in which LR cells of one hemisphere might serve to influence the activity of the contralateral hemisphere. However, it is also possible that LR axons continue onto other brain regions, as the RSC projects to several areas involved in memory and spatial navigation processing (van Groen & Wyss, 1990). A major challenge in the field will be to identify precise molecular markers for LR cells to help in identifying their cell-type-specific projections.

### **Implications of dominant inhibition of LR neurons from neighboring FS cells**

In contrast to the lack of local connectivity of LR cells, there is dense connectivity between FS cells and their neighboring excitatory neurons, with the probability of FS-to-LR connectivity reaching 52% (Figure 6), higher than that reported in other regions of the neocortex. For example, connectivity probabilities between FS and pyramidal neurons in superficial layers of the mouse visual cortex was reported as roughly 35%, of the rat visual cortex as 46.5%, of the mouse somatosensory cortex as only 19%, and of the rat barrel cortex as 44% (Beierlein et al., 2003; Jiang et al., 2015; Packer and Yuste, 2011; Yoshimura and Callaway, 2005). This, coupled with the complete lack of local excitatory connections onto LR cells (0%; Figure 6), indicates that the superficial layers of the RSG are a network dominated by strong local inhibition. Therefore, the activity of LR neurons in the superficial RSG is likely to be strongly influenced by feedforward inhibition from neighboring FS neurons.

In strong concordance with our results, a recent study quantifying the response of pyramidal neurons in the superficial RSD to contralateral stimulation has shown that layer 2/3 is characterized by inhibition-dominated feed-forward dynamics (Gejjo-barrientos et al., 2019; Sempere-Ferràndez et al., 2018). Also, in response to photostimulation of subicular axons which project extensively to layer 3 of the RSC, the firing of superficial pyramidal neurons is dominated by strong feed-forward inhibition coming from local interneurons (Corcoran et al., 2018). Therefore, similar to the other cortical regions (Avermann et al., 2012; Mateo et al., 2011), the superficial RSG could implement a sparse neuronal code dominated by local inhibition from interneurons. Given the well-known role of the RSC in memory and spatial navigation related functions, such sparse population codes can greatly boost the pattern storage and recognition capabilities of the system (Marr, 1971). Indeed, sparse neuronal codes representing sequential, place-cell like firing have been reported in the neurons of the superficial RSC during spatially-guided movements (Mao et al., 2017). Our results start to explain how the local cells and circuitry of the superficial retrosplenial cortex can support these unique computational functions.

## REFERENCES

- Alexander AS, Nitz DA. 2015. Retrosplenial cortex maps the conjunction of internal and external spaces. *Nat Neurosci* 18 :1143–1151.
- Avermann M, Tomm C, Mateo C, Gerstner W, Petersen CCH. 2012. Microcircuits of excitatory and inhibitory neurons in layer 2/3 of mouse barrel cortex. *J Neurophysiol* 107 :3116–3134. doi:10.1152/jn.00917.2011
- Beierlein M, Gibson JR, Connors BW. 2003. Two Dynamically Distinct Inhibitory Networks in Layer 4 of the Neocortex. *J Neurophysiol* 90 :2987–3000. doi:10.1152/jn.00283.2003
- Bottini G, Cappa S, Geminiani G, Sterzi R. 1990. Topographic disorientation-A case report. *Neuropsychologia* 28 :309–312. doi:10.1016/0028-3932(90)90024-I
- Buckley MJ, Mitchell AS. 2016. Retrosplenial Cortical Contributions to Anterograde and Retrograde Memory in the Monkey. *Cereb Cortex* . doi:10.1093/cercor/bhw054
- Cho J, Sharp PE. 2001. Head direction, place, and movement correlates for cells in the rat retrosplenial cortex. *Behav Neurosci* 115 :3–25. doi:10.1037/0735-7044.115.1.3
- Chrastil ER. 2018. Heterogeneity in human retrosplenial cortex: A review of function and connectivity. *Behav Neurosci* .
- Corcoran KA, Yamawaki N, Radulovic J, Shepherd GMG, Guedea AL. 2018. Differential Contributions of Glutamatergic Hippocampal Retrosplenial Cortical Projections to the Formation and Persistence of Context Memories. *Cereb Cortex* 1–9. doi:10.1093/cercor/bhy142
- Cruikshank SJ, Ahmed OJ, Stevens TR, Patrick SL, Gonzalez AN, Elmaleh M, Connors BW. 2012. Thalamic control of layer 1 circuits in prefrontal cortex. *J Neurosci* 32 :17813–17823.
- Epstein RA. 2008. Parahippocampal and retrosplenial contributions to human spatial navigation. *Trends Cogn Sci* 12 :388–396.
- Geijo-barrientos E, Martinez S, Sempere-ferrandez A. 2019. Synaptic mechanisms underlying the intense firing of neocortical layer 5B pyramidal neurons in response to cortico-cortical inputs. *Brain Struct Funct* 1–14. doi:10.1007/s00429-019-01842-8

Heilman KM, Sybert GW. 1977. Korsakoff's syndrome resulting from bilateral fornix lesions. *Neurology* 27 :490.

Ino T, Doi T, Hirose S, Kimura T, Ito J, Fukuyama H. 2007. Directional Disorientation Following Left Retrosplenial Hemorrhage: A Case Report with fMRI Studies. *Cortex* 43 :248–254.

Irnside R, Guttmacher M. 1929. The corpus callosum and its tumours. *Brain* 52 :442–483.

Jiang X, Shen S, Cadwell CR, Berens P, Sinz F, Ecker AS, Patel S, Tolias AS. 2015. Principles of connectivity among morphologically defined cell types in adult neocortex. *Science (80- )* 350 . doi:10.1126/science.aac9462

Keene CS, Bucci DJ. 2008. Contributions of the retrosplenial and posterior parietal cortices to cue-specific and contextual fear conditioning. *Behav Neurosci* 122 :89–97.

Kurotani T, Miyashita T, Wintzer M, Konishi T, Sakai K, Ichinohe N, Rockland KS. 2013. Pyramidal neurons in the superficial layers of rat retrosplenial cortex exhibit a late-spiking firing property. *Brain Struct Funct* 218 :239–254. doi:10.1007/s00429-012-0398-1

Maguire E. 2001. The retrosplenial contribution to human navigation: a review of lesion and neuroimaging findings. *Scand J Psychol* 42 :225–238.

Mao D, Kandler S, McNaughton BL, Bonin V. 2017. Sparse orthogonal population representation of spatial context in the retrosplenial cortex. *Nat Commun* 8 :243. doi:10.1038/s41467-017-00180-9

Marr D. 1971. Simple Memory: A Theory for Archicortex. *Philos Trans R Soc B Biol Sci* 262 :23–81. doi:10.1098/rstb.1971.0078

Mateo C, Avermann M, Gentet LJ, Zhang F, Deisseroth K, Petersen CCH. 2011. In Vivo Optogenetic Stimulation of Neocortical Excitatory Neurons Drives Brain-State-Dependent Inhibition. *Curr Biol* 21 :1593–1602. doi:10.1016/j.cub.2011.08.028

Michael JW, Van Groen T, Sripanidkulchai K. 1990. Dendritic bundling in layer I of granular retrosplenial cortex: Intracellular labeling and selectivity of innervation. *J Comp Neurol* 295 :33–42. doi:10.1002/cne.902950104

Osawa A, Maeshima S, Kunishio K. 2007. Topographic disorientation and amnesia due to cerebral hemorrhage in the left retrosplenial region [2]. *Eur Neurol* . doi:10.1159/000109572

Packer AM, Yuste R. 2011. Cellular/Molecular Dense, Unspecific Connectivity of Neocortical Parvalbumin-Positive Interneurons: A Canonical Microcircuit for Inhibition? *J Neurosci* 31 . doi:10.1523/JNEUROSCI.3131-11.2011

Sempere-Ferrandez A, Andres-Bayon B, Geijo-Barrientos E. 2018. Callosal responses in a retrosplenial column. *Brain Struct Funct* 223 :1051–1069. doi:10.1007/s00429-017-1529-5

Shine JP, Valdes-Herrera JP, Hegarty M, Wolbers T. 2016. The Human Retrosplenial Cortex and Thalamus Code Head Direction in a Global Reference Frame. *J Neurosci* 36 :6371.

Sigwald EL, Genoud ME, Giachero M, de Olmos S, Molina VA, Lorenzo A. 2016. Selective neuronal degeneration in the retrosplenial cortex impairs the recall of contextual fear memory. *Brain Struct Funct* 221 :1861–1875. doi:10.1007/s00429-015-1008-9

Sudhakar SK, Hong S, Raikov I, Publio R, Lang C, Close T, Guo D, Negrello M, De Schutter E. 2017. Spatiotemporal network coding of physiological mossy fiber inputs by the cerebellar granular layer. *PLoS Comput Biol* 13 :e1005754. doi:10.1371/journal.pcbi.1005754

Sugar J, Witter M, van Strien N, Cappaert N. 2011. The retrosplenial cortex: Intrinsic connectivity and connections with the (para)hippocampal region in the rat. An interactive connectome. *Front Neuroinform* 5 . doi:10.3389/fninf.2011.00007

Takahashi N, Kawamura M, Shiota J, Kasahata N, Hirayama K. 1997. Pure topographic disorientation due to right retrosplenial lesion. *Neurology* 49 :464–469.

Todd TP, Bucci DJ. 2015. Retrosplenial Cortex and Long-Term Memory: Molecules to Behavior. *Neural Plast* 2015 :9. doi:10.1155/2015/414173

Todd TP, DeAngeli NE, Jiang MY, Bucci DJ. 2017. Retrograde amnesia of contextual fear conditioning: Evidence for retrosplenial cortex involvement in configural processing. *Behav Neurosci* 131 :46–54. doi:10.1037/bne0000183

Todd TP, Meyer HC, Bucci DJ. 2015. Contribution of the retrosplenial cortex to temporal discrimination learning. *Hippocampus* 25 :137–141. doi:10.1002/hipo.22385

Valenstein E, Bowers D, Verfaellie M, Heilman KM, Day A, Watson RT. 1987. Retrosplenial amnesia. *Brain* 110 :1631–1646.

van Groen T, Kadish I, Wyss JM. 2004. Retrosplenial cortex lesions of area Rgb (but not of area Rga) impair spatial learning and memory in the rat. *Behav Brain Res* 154 :483–491.

van Groen T, Michael Wyss J. 1990. Connections of the retrosplenial granular a cortex in the rat. *J Comp Neurol* 300 :593–606. doi:10.1002/cne.903000412

Van Groen T, Wyss JM. 2003. Connections of the retrosplenial granular b cortex in the rat. *J Comp Neurol* 463 :249–263. doi:10.1002/cne.10757

Vann SD, Kristina Wilton LA, Muir JL, Aggleton JP. 2003. Testing the importance of the caudal retrosplenial cortex for spatial memory in rats. *Behav Brain Res* 140 :107–118. doi:http://dx.doi.org/10.1016/S04328(02)00274-7

Vedder LC, Miller AMP, Harrison MB, Smith DM. 2016. Retrosplenial cortical neurons encode navigational cues, trajectories and reward locations during goal directed navigation. *Cereb Cortex* . doi:10.1093/cercor/bhw192

Wyss JM, Van Groen T. 1992. Connections between the retrosplenial cortex and the hippocampal formation in the rat: A review. *Hippocampus* 2 :1–11. doi:10.1002/hipo.450020102

Yamawaki N, Li X, Lambot L, Ren LY, Radulovic J, Shepherd GM. 2019. Long-range inhibitory intersection of a retrosplenial thalamocortical circuit by apical tuft-targeting CA1 neurons. *Nat Neurosci* 1. doi:10.1101/427179

Yoshimura Y, Callaway EM. 2005. Fine-scale specificity of cortical networks depends on inhibitory cell type and connectivity. *Nat Neurosci* 8 . doi:10.1038/nn1565